

Modeling enantiomeric separations as an interfacial process using amylose tris(3,5-dimethylphenyl carbamate) (ADMPC) polymers coated on amorphous silica

Xiaoyu Wang,[‡] Cynthia J. Jameson,[§] and Sohail Murad ^{‡ *}

[‡]Department of Chemical Engineering, Illinois Institute of Technology, 10 West 33rd Street, Perlstein Hall, Chicago, Illinois 60616, United States

[§]Department of Chemistry, University of Illinois at Chicago, 845 W. Taylor St. Chicago, Illinois 60607, United States

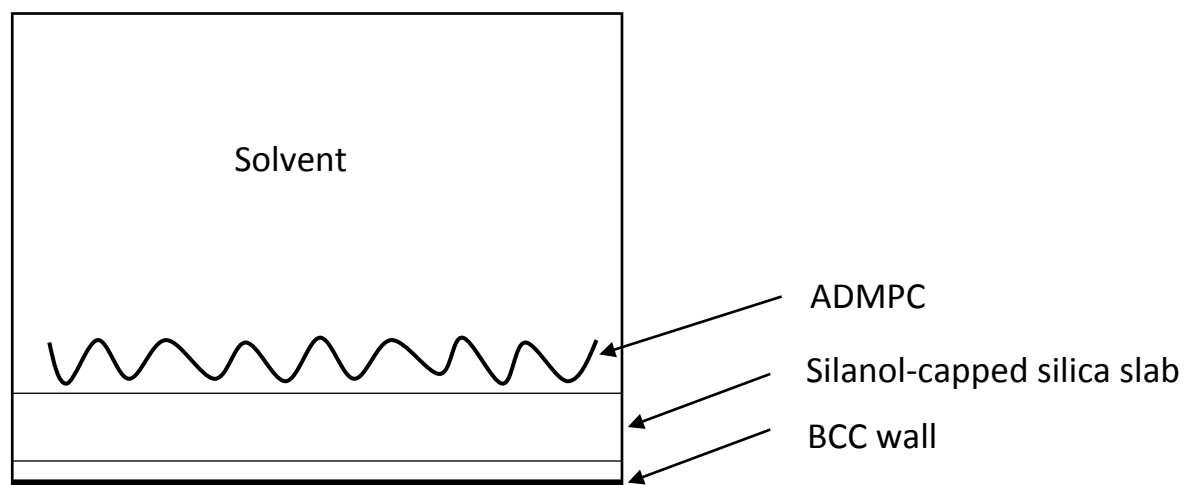


Fig. S1. System arrangement for equilibrating the polymer strands on the amorphous silica in the presence of solvent

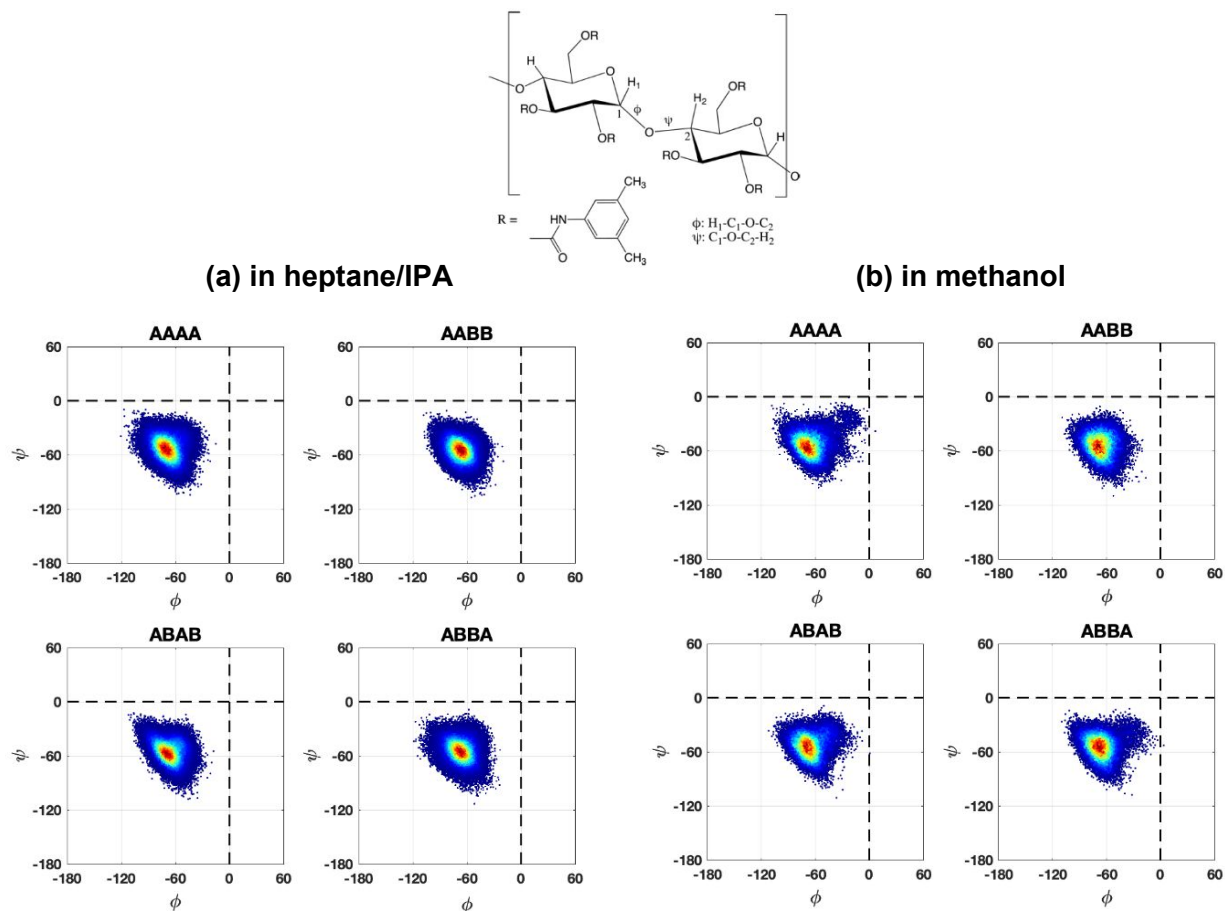


Fig S2. Ramachandran maps of dihedral angles of the glycoside bond between adjacent monomers of the four 18-mers of ADMPC on silanol-capped silica (a) in hep/IPA and (b) in methanol, in various parallel/antiparallel arrangements. The colors from blue to red represent the density of the data points going from low to high. Of the four quadrants $(\phi, \psi) = -180^\circ$ to $+180^\circ$, we only show the populated quadrant.

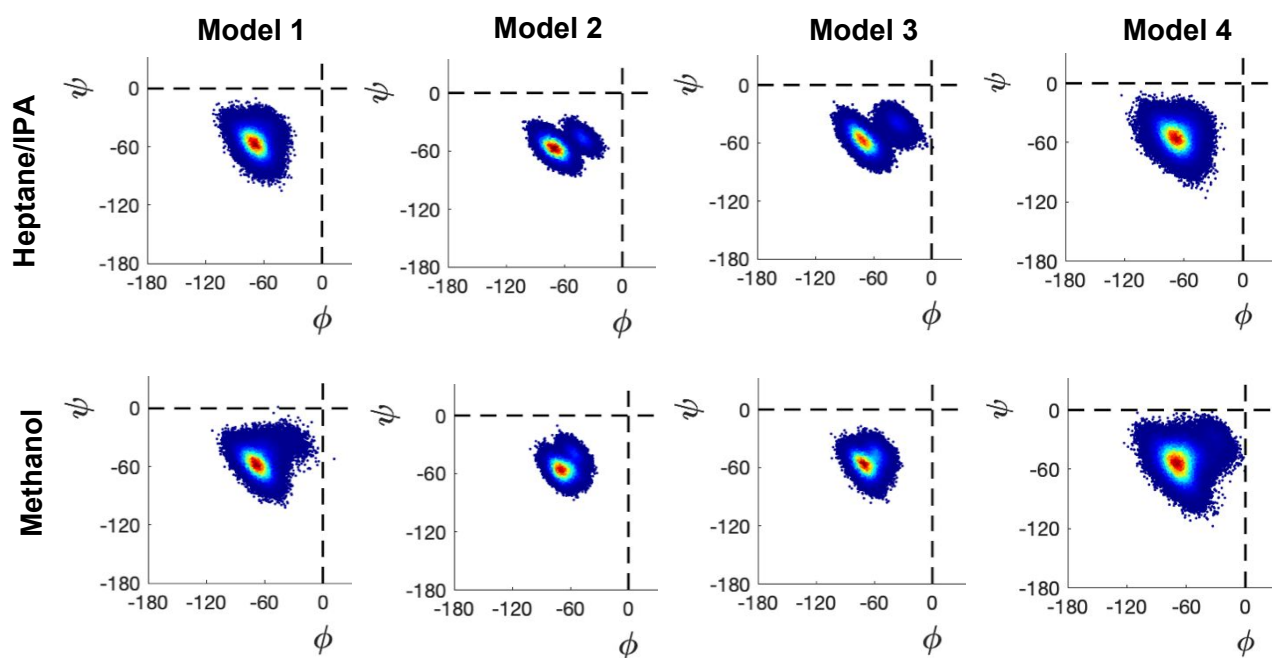


Fig. S3. Maps of dihedral angles of the glycoside bond between adjacent monomers of the four 18-mers of ADMPC on silanol-capped silica in methanol (or hep/IPA), (the current Model 4) all arrangements combined, compared with previous Models 1, 2, and 3, all of which are a single ADMPC 12-mer strand equilibrated in the solvent system, completely unrestrained, slightly restrained, and only backbone atoms restrained, respectively. The colors from blue to red represent the density of the data points going from low to high. Of the four quadrants $(\phi, \psi) = -180^\circ$ to $+180^\circ$, we only show the populated quadrant.

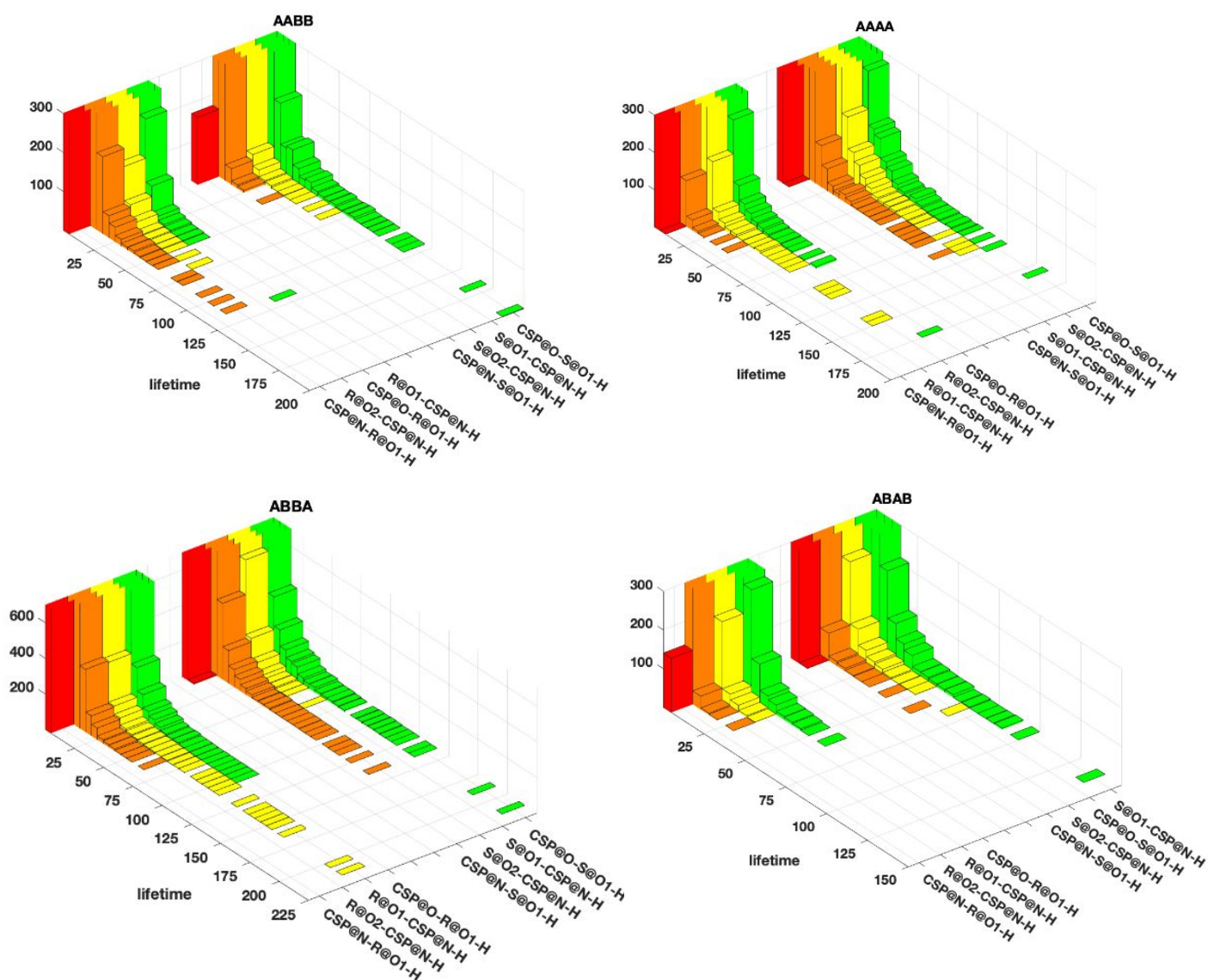


Fig. S4. Distribution of lifetimes (ps) of hydrogen bonds between S or R enantiomers and ADMPC on silica for) benzoin in hep/IPA for each of the donor-acceptor pairs. CSP@O and CSP@N denote the acceptor oxygen and nitrogen sites, and CSP@N-H denotes the donor site in the chiral stationary phase ADMPC strands on silica. Likewise, S@O1 and R@O1 denote the acceptor sites while S@O1-H and R@O1-H denote the donor sites on the S and R enantiomers, respectively. These are the sites identified in Fig. 1 for benzoin and ADMPC. We show the results for various parallel and anti-parallel arrangements of polymer strands on the silica. The y axis counts the number of incidences over the entire trajectory; the very high counts for the very short lifetimes are cut off in this display.

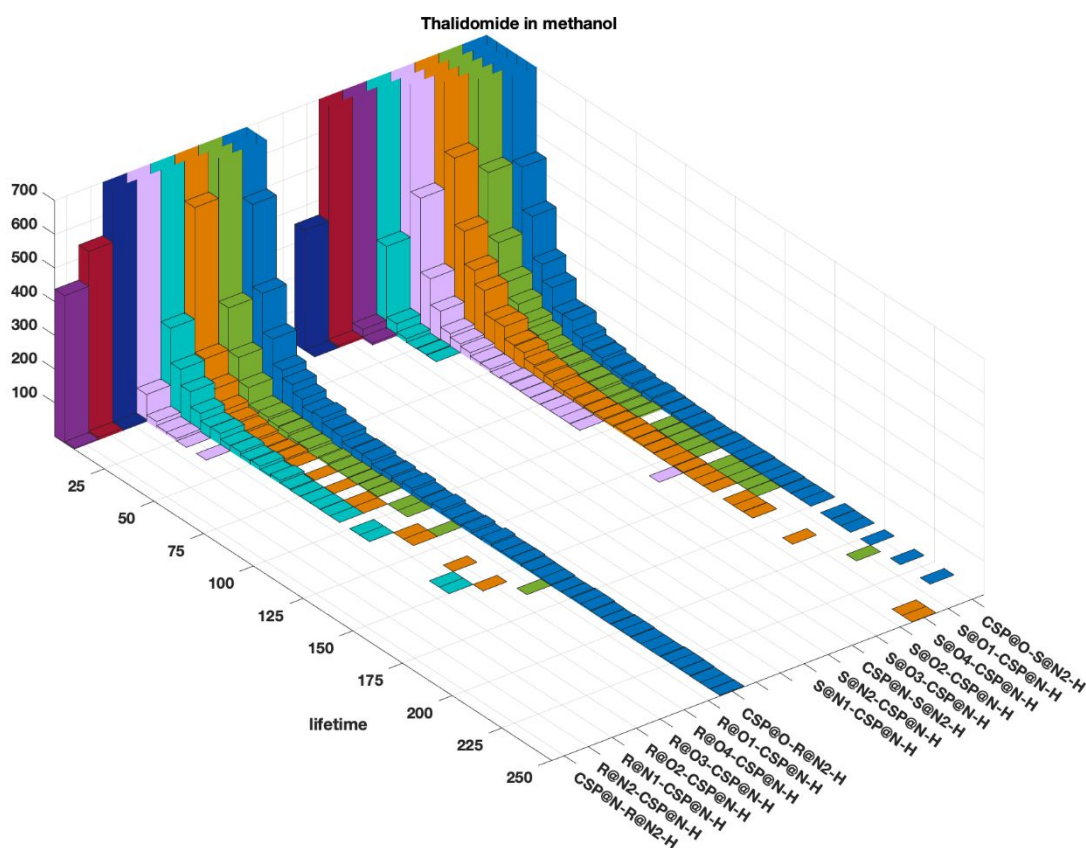


Fig. S5. Distribution of lifetimes (ps) of hydrogen bonds between S or R enantiomers and ADMPC on silica for thalidomide in methanol. CSP@O and CSP@N denote the acceptor oxygen and nitrogen sites, and CSP@N-H denotes the donor site in the chiral stationary phase ADMPC strands on silica. Likewise, S@O1, S@O2, S@O3, S@O4, S@N1, S@N2, and R@O1, R@O2, R@O3, R@O4, R@N1, R@N2 denote the acceptor sites while S@N2-H and R@N2-H denote the donor sites on the S and R enantiomers, respectively. These are the sites identified in Fig. 1 for thalidomide and ADMPC. The y axis counts the number of incidences over the entire trajectory, summed over all four parallel/antiparallel arrangements shown in Fig. 3; the very high counts for the very short lifetimes are cut off in this display.

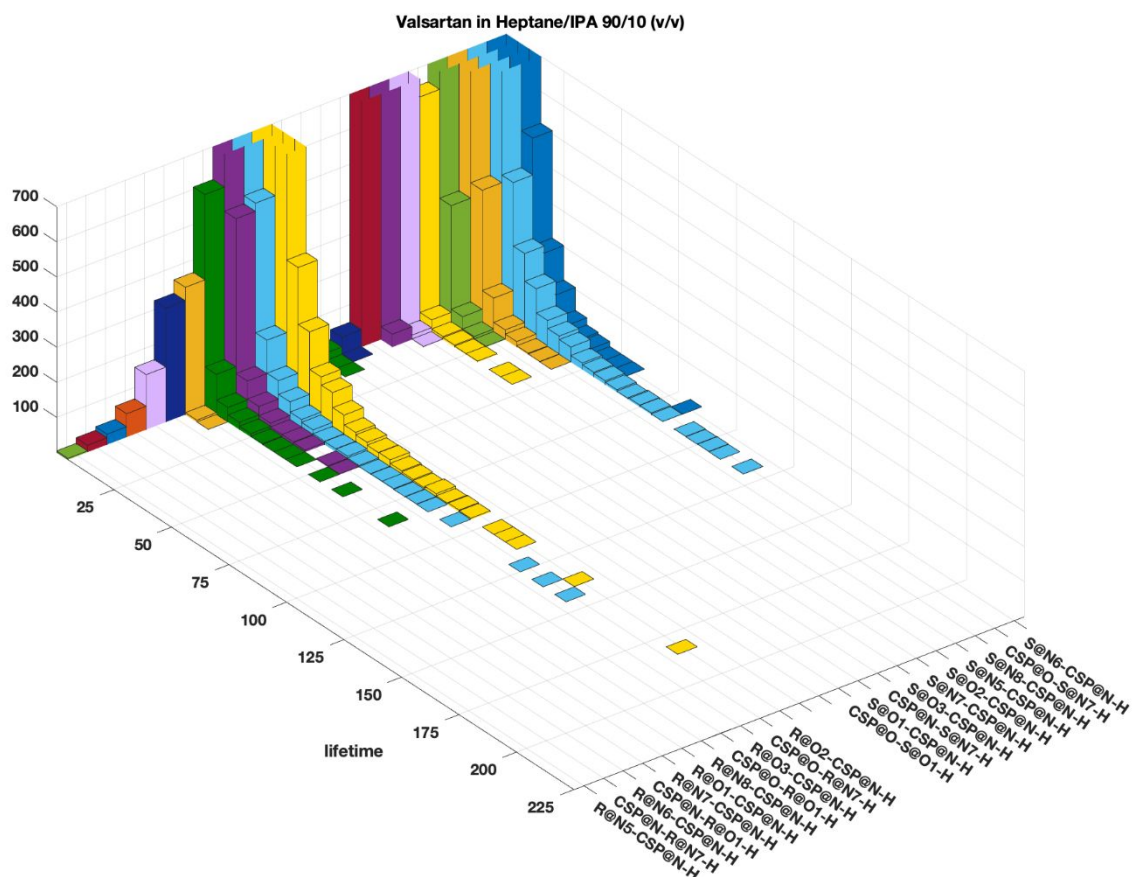


Fig. S6. Distribution of lifetimes (ps) of hydrogen bonds between S or R enantiomers and ADMPC on silica for valsartan in hep/IPA. CSP@O and CSP@N denote the acceptor oxygen and nitrogen sites, and CSP@N-H denotes the donor site in the chiral stationary phase ADMPC strands on silica. Likewise, S@O1, S@O2, S@O3, S@N5, S@N6, S@N7, S@N8, and R@O1, R@O2, R@O3, R@N5, R@N6, R@N7, R@N8 denote the acceptor sites while S@O1-H, S@N7-H and R@O1-H, R@N7-H denote the donor sites on the S and R enantiomers, respectively. These are the sites identified in Fig. 1 for valsartan and ADMPC. The y axis counts the number of incidences over the entire trajectory, summed over all four parallel/antiparallel arrangements shown in Fig. 3; the very high counts for the very short lifetimes are cut off in this display.

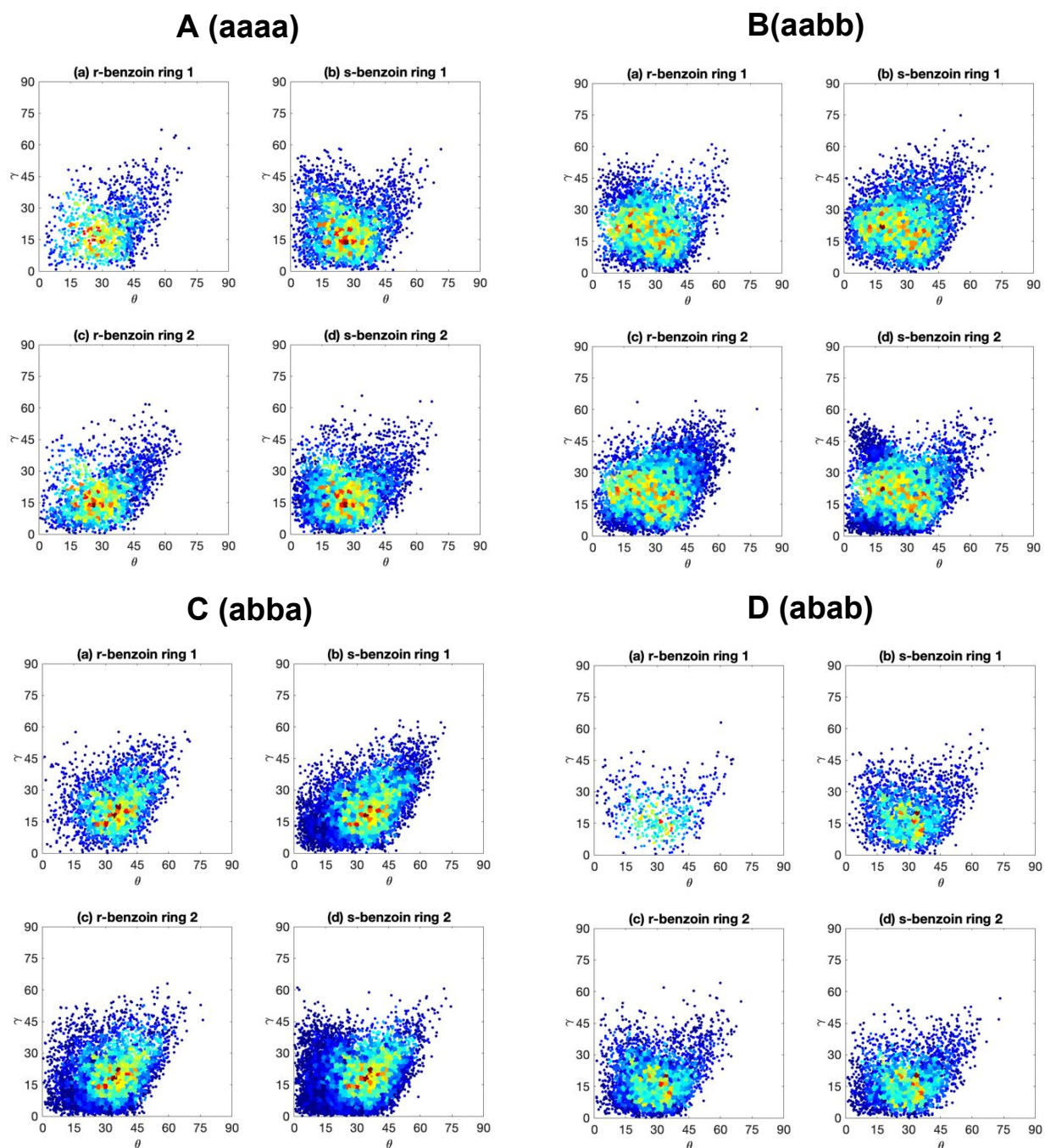


Fig. S7. Map of the angles describing the distribution of relative orientations of the phenyl rings (γ = vertical axis, θ = horizontal axis), found for distances R_{cen} less than 4.4 Å between the center of the phenyl ring#1 and ring#2 of the benzoin molecule and the closest ADMPC phenyl ring, using the present model in hep/IPA. The colors from blue to red represent the density of the data points going from low to high. The results are based on snapshots uniformly taken from a 100 ns trajectory, (a) for the R enantiomer (b) for the S enantiomer for ring #1, (c) for the R enantiomer (d) for the S enantiomer for ring #2. The presentation is the same as for all arrangements shown in Figure 9. Here we show: (A) the (aaaa) arrangement, (B) (aabb) arrangement, (C) the (abba) arrangement, (D) the (abab) arrangement.

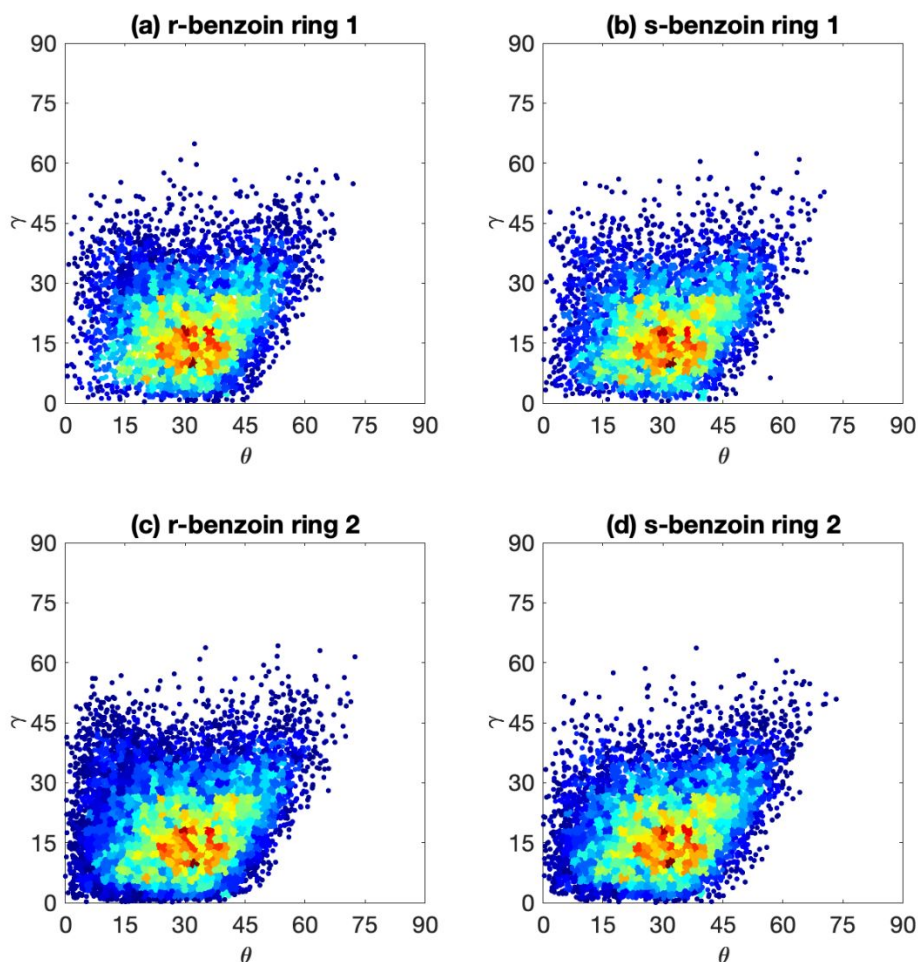


Fig. S8. Map of the angles describing the distribution of relative orientations of the phenyl rings (γ = vertical axis, θ = horizontal axis), found for distances R_{cen} less than 4.4 Å between the center of the phenyl ring#1 and ring#2 of the benzoin molecule and the closest ADMPC phenyl ring, as in Fig. 9, but for a free-floating 12-mer in solution (Model 1). The most probable (γ, θ) angle values are much more spread out than for the ring-ring interactions between benzoin and the ADMPC strands on amorphous silica slab. The plots are almost indistinguishable for the S vs. R enantiomers, an indication of the lower chiral selectivity of the Model 1 ADMPC.